AGU PUBLICATIONS

JGR

Journal of Geophysical Research: Atmospheres

RESEARCH ARTICLE
10.1002/2016JD025611

Key Points:
- A proper new scaling is introduced in the complementary relationship of evaporation
- An upper limit is defined for the Penman-equation evaporation rate
- A model-independent new method is developed for obtaining the Priestley-Taylor parameter value

Correspondence to:
J. Szilagyi,
jszilagyi1@unl.edu

Citation:
Szilagyi, J., R. Crago, and R. Qualls (2016), A calibration-free formulation of the complementary relationship of evaporation for continental-scale hydrology, *J. Geophys. Res. Atmos.*, *122*, doi:10.1002/2016JD025611.

Received 3 JUL 2016
Accepted 19 DEC 2016
Accepted article online 22 DEC 2016

A calibration-free formulation of the complementary relationship of evaporation for continental-scale hydrology

Jozsef Szilagyi[1,2], Richard Crago[3], and Russell Qualls[4]

[1]Department of Hydraulic and Water Resources Engineering, Budapest University of Technology and Economics, Budapest, Hungary, [2]Conservation and Survey Division, School of Natural Resources, University of Nebraska–Lincoln, Lincoln, Nebraska, USA, [3]Department of Civil and Environmental Engineering, Bucknell University, Lewisburg, Pennsylvania, USA, [4]Department of Biological Engineering, University of Idaho, Moscow, Idaho, USA

Abstract An important scaling consideration is introduced into the formulation of the complementary relationship (CR) of land surface evapotranspiration (ET) by specifying the maximum possible evaporation rate (E_{pmax}) of a small water body (or wet patch) as a result of adiabatic drying from the prevailing near-neutral atmospheric conditions. In dimensionless form the CR therefore becomes $y_B = f(\frac{E_{pmax}-E_p}{E_{pmax}-E_w}x_B) = f(X) = 2X^2 - X^3$, where $y_B = \mathrm{ET}/E_p$, $x_B = E_w/E_p$. E_w is the wet-environment evaporation rate as given by the Priestley-Taylor equation, E_p is the evaporation rate of the same small wet surface for which E_{pmax} is specified and estimated by the Penman equation. With the help of North American Regional Reanalysis data, the CR this way yields better continental-scale performance than earlier, calibrated versions of it and is on par with current land surface model results, the latter requiring vegetation, soil information and soil moisture bookkeeping. Validation has been performed by Parameter-Elevation Regressions on Independent Slopes Model precipitation and United States Geological Survey runoff data. A novel approach is also introduced to calculate the value of the Priestley-Taylor parameter to be used with continental-scale data, making the new formulation of the CR completely calibration free.

1. Introduction

Land-atmosphere interactions play an important role in forming the regional climate [*Diro et al.*, 2014] by partitioning the energy balance of the land surface (R_n) into sensible (H) and latent (LE) heat fluxes [*Berbery et al.*, 2003]. Accurate determination of these fluxes over extended time intervals and/or extensive areas is crucial not only for climate modeling [*Phillips and Klein*, 2013; *Diro et al.*, 2014] but also for hydroclimatological predictions and simulations [*Zhang et al.*, 2007, 2008; *Swenson and Lawrence*, 2014], as well as long-term and/or large-scale water management operations including drought monitoring [*Sheffield and Wood*, 2007; *Xia et al.*, 2014] and flood alleviation [*Lavers et al.*, 2012]. While remote sensing-based flux estimation methods, especially for LE, are developing rapidly (for a review, see *Wang and Dickinson* [2012]), reanalysis-based methods [*Chen et al.*, 1997; *Koster and Suarez*, 1996; *Liang et al.*, 1994; *Mesinger et al.*, 2006; *Lavers et al.*, 2012] stay relevant because of their longer temporal coverage, their insensitivity to cloud cover, and because they may form part of remote sensing-based LE estimation techniques [*Szilagyi et al.*, 2011; *Wu et al.*, 2014]. Reanalysis data are often considered as the best representation of reality for spatially distributed, long-term analyses and simulations, since they combine measurements with modeling results by taking into account the errors in both. The North American Regional Reanalysis (NARR) data set [*Mesinger et al.*, 2006] provides an improvement in continental-scale reanalyses due to its finer resolution (i.e., 32 km), its state-of-the-art land surface model (LSM) component, and the assimilation of observed precipitation for the North American continent and adjacent oceans over the past 35 years [*Sheffield et al.*, 2012]. The LSMs provide H and LE fluxes, typically employing variations of the Penman-Monteith equation [*Monteith*, 1965] for the latter over land areas, requiring soil, and vegetation information to perform soil moisture budgeting. Considering the typically large heterogeneity in soil type, thickness, water drainage [*Campoy et al.*, 2013], layering, vegetation cover, and rooting depth, the ensuing LSM-derived LE fluxes may contain a relatively high degree of uncertainty. Such noticeable differences in LE rates [*Berbery et al.*, 2003; *Sheffield et al.*, 2012] thus give rise to the need for an alternative formulation of the evapotranspiration rates (ET, typically given in units of water depth per unit time), preferably by a method that inherently accounts for the integrated effects of the soil/land/vegetation interface. These independently derived ET rates then may be used for calibration and/or validation of the different LSM formulations.

Introduced by *Bouchet* [1963], the complementary relationship (CR) of evaporation has presented itself an attractive tool for estimating land surface ET rates at a regional scale due to its minimal data requirement. However, it gained wide-spread attention only around the turn of the millennium when *Brutsaert and Parlange* [1998] explained the evaporation paradox [*Peterson et al*., 1995] of a seemingly failing global water cycle in a warmer world with its help. They pointed out that a decrease in global pan evaporation rates over land is in fact a tell-tale sign of an accelerated hydrologic cycle as expected from global warming, since air enriched in moisture via increased land ET rates in fact exerts less evaporative demand measured by the pans.

The core idea of the CR is that the moisture content of the air (as effect), averaged over a suitable period, is related to the ET rate (as cause) of the underlying homogeneous land. In the 1960s this was a new claim since up until that time actual ET rates were typically related to the soil moisture content by which a maximum attainable ET rate (under the prevailing atmospheric conditions), called potential evaporation, E_p, was scaled down [see, e.g., *Thornthwaite and Mather*, 1955]. The CR realizes that E_p is indeed an indicator of the moisture content of the air, since the larger the E_p rate the drier the air (under the prevailing atmospheric conditions), the latter quantified by either the relative humidity (i.e., ratio of actual to saturation vapor pressure) or the vapor pressure deficit (i.e., difference in saturation and actual vapor pressure), the latter appearing in the equation for E_p below.

Notice that scale is very important in the CR because self-adjustment of the atmospheric moisture content to the ET rate of the land surface is not abrupt at discontinuities of land surface properties. In fact, *Davenport and Hudson* [1967] and *Lang et al*. [1974] showed that such an adjustment is on the order of about 10^3 m. As a consequence, this scale (i.e., 1 km) is the highest resolution the CR can be applied at with gridded data sets. There is also a temporal resolution to be considered with the routine application of the CR since large-scale weather fronts can easily disturb the equilibrium ET rate of the land-atmosphere system by bringing air masses over the land with a moisture signature decoupled from the underlying surface, at least for a while. Therefore, *Morton* [1983] cautioned not to use the CR routinely for periods shorter than about 5 days, which thus forms the lower limit of temporal averaging of the input variables required by the CR when applied for extended periods and over a wide range of climate, as in this study.

As a further demonstration of the importance of scale, a second maximum attainable ET rate must be defined, valid at the scale of the CR (i.e., larger than about 1 km), called wet-environment ET rate, E_w [*Priestley and Taylor*, 1972], which is the ET rate of the homogeneous surface when soil moisture is not limiting. The fact that $E_w \leq E_p$ originates from E_p being valid at a scale of about 1–100 m and thus incapable of significantly affecting the humidity and temperature of the overpassing air. E_p can be measured by different ways, for example, by sunken evaporation pans, irrigated lysimeters, or calculated by the *Penman* [1948] equation. (Aboveground pans suffer from an elevated height which affect air-flow around and over them as well as from an increased area, due to their metallic side, through which additional exchange of energy with the environment takes place.) The three ET rates ($\mathrm{ET} \leq E_w \leq E_p$) become equal under regionally wet conditions, since then the same near-saturated air properties exert the ET response of the surface, independent of scale.

1.1. Equations of Wet-Surface Evaporation

It is important to point out that *Priestley and Taylor* [1972] estimated E_w under actually wet environmental conditions when air temperature, T_w, is affected by the cooling effect of regional evaporation; therefore, $T_w \leq T_a$, the latter denoting the typically "nonwet" actual air temperature, which occasionally may come from wet environmental conditions allowing for the equality

$$E_w = \alpha \frac{\Delta(T_w)}{\Delta(T_w) + \gamma} R_n. \tag{1}$$

Here $\Delta(T_w)$ is the slope of the saturation vapor pressure curve at T_w, $\gamma[= c_p p/(0.622\, L)]$ is the psychrometric constant, where c_p is the specific heat of air at constant air pressure (p), L is the latent heat of vaporization (2.47×10^6 J kg^{-1} at 15°C) for water, and R_n the net radiation at the surface. For convenience R_n and E_w are specified in the same units of water depth per unit time (e.g., mm d^{-1}), similar to the customary form of the *Penman* [1948] equation (3) below. The coefficient α is called the Priestley-Taylor parameter, and it

accounts for the ET-enhancing effect of large-scale advection [*Brutsaert*, 1982; *de Bruin*, 1983; *Culf*, 1994; *Lhomme*, 1997; *Heerwaarden et al*., 2009] having typical values within the range of 1.1 to 1.32.

As *Huntington et al*. [2011] demonstrated, the difference between the two temperatures, T_w and T_a, may reach 10 K in hot, arid regions, making necessary the approximation of T_w when (1) is employed under typically subhumid environmental conditions (i.e., when $T_a > T_w$) [*Ma et al*., 2015]. Estimation of T_w is a two-step process, requiring first the temperature of the wet surface, T_{ws}. Specification of the Bowen ratio (B_o) between H and LE ($= 8.64 \times 10^{-7} L\rho$ET, where ρ is water density), written for a small wet patch (for which E_p is valid), yields an implicit equation for T_{ws} [*Szilagyi*, 2014a, 2015; *Szilagyi and Jozsa*, 2008; *Huntington et al*., 2011; *Szilagyi and Schepers*, 2014] since R_n, T_a, and the dew point temperature (T_d) are typically known and E_p is either measured by a sunken pan or irrigated lysimeter or specified by the Penman equation below

$$B_o = \frac{H}{\mathrm{LE}} \approx \frac{R_n - E_p}{E_p} \approx \gamma \frac{T_{ws} - T_a}{e^*(T_{ws}) - e^*(T_d)}. \tag{2}$$

The saturation vapor pressure, e^* (hPa), at any temperature, T (°C), can be obtained by, e.g., the Tetens equation as $e^* = 6.108 \exp[17.23\,T/(237.3 + T)]$. Note that T_{ws} is the same over a small wet patch as over a regional one and is unaffected by adiabatic cooling or warming of the drying surface around it for the given R_n and mean horizontal wind (u) conditions [*Szilagyi and Schepers*, 2014]. (Adiabatic conditions here mean that the sum of H and LE for a parcel of air in contact with the surface equals $8.64 \times 10^{-7} L\rho R_n$ which is held constant during the warming or cooling.) As a consequence, E_w also stays constant (i.e., a constant T_w follows from a constant T_{ws} and unchanging wind) under similar adiabatic changes.

E_p can be obtained from the *Penman* [1948] equation in mm d^{-1}, the same as R_n, as

$$E_p = \frac{\Delta(T_a)}{\Delta(T_a) + \gamma} R_n + \frac{\gamma}{\Delta(T_a) + \gamma} f_u [e^*(T_a) - e^*(T_d)]. \tag{3}$$

Here f_u (in mm d^{-1} hPa^{-1}) is an empirical wind function, traditionally written as $f_u = 0.26(1 + 0.54u_2)$, where u_2 is the mean horizontal wind speed in m s^{-1} at 2 m above the ground and e^* is in hPa. Notice that (i) $e^*(T_d)$ equals actual vapor pressure, e_a; (ii) $e^*(T_a) - e_a$ is called the vapor pressure deficit, VPD. It is also important to note that in the Penman (unlike in the Priestley-Taylor) equation, the actual, subhumid air temperature, T_a, is employed, since the small wet patch cannot alter the prevailing atmospheric conditions around it.

As an alternative, T_{ws} can also be obtained from the Penman-Monteith equation [*Monteith*, 1965] in combination with the expression he obtained for T_{ws} [*Monteith*, 1981] via parameterization of the elusive aerodynamic resistance term (included in both equations) by the help of the Penman equation. *Szilagyi* [2014a] obtained the so-derived T_{ws}, denoted by T_{wsM}, as

$$T_{wsM} = T_{wb} + \frac{\gamma Q_n VPD}{(\Delta^{wb} + \gamma)(aQ_n + bf_u VPD)} \tag{4}$$

with a and b defined as

$$a = \frac{\Delta(\Delta^{wb} + \gamma) - \Delta^{wb}(\Delta + \gamma)}{\Delta + \gamma}; \quad b = \frac{c\gamma(\Delta^{wb} + \gamma)}{\Delta + \gamma} \tag{5}$$

where T_{wb} is the wet-bulb temperature, the lowest temperature of the air attainable by adiabatic cooling when R_n is zero at the evaporating surface and LE is sustained solely by H, directed from the air toward the small wet surface. Δ^{wb} is shorthand for $\Delta(T_{wb})$ and c ($= 28.94$ Wd mm^{-1} m^{-2}) is a coefficient used to transform R_n in mm d^{-1} into flux units of W m^{-2}, denoted by Q_n in (4). *Szilagyi* [2014a] found that T_{wsM} is typically within 1 K of T_{ws} and tends to be higher than the latter.

Over extensive wet surfaces where equilibrium profiles (meaning monotonically decreasing values of T_a and e_a by distance from the ground) of the fluxes develop and for which (1) is valid, T_w is confined within T_{wb} and T_{ws} (see (4)), i.e., $T_{wb} \le T_w \le T_{ws}$, and is also confined within $T_{wb} \le T_w \le T_a$; therefore, $T_{wb} \le T_w \le \min(T_{ws}, T_a)$ can be written where "min" denotes the smaller of the two values. There are two simple choices for the approximation of T_w. (a) T_{ws} (meaning either estimate, (2) or (4), of T_{ws}) can serve as a proxy for the unknown T_w required by (1) since over extensive wet/water surfaces the vertical gradient of the equilibrium air temperature profile is small because ET is much more effective in cooling the surface than sensible heat fluxes due to

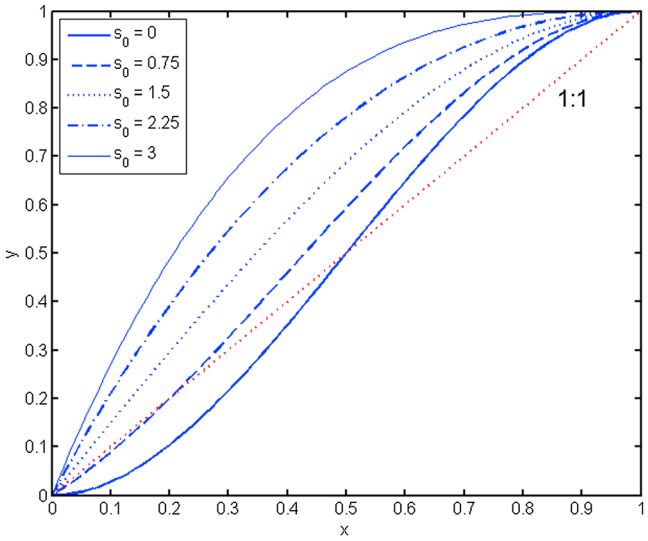

Figure 1. Equation (7) for selected values of s_0. $y = ET/E_w$, $x = e_a/e^*(T_w)$.

the large value of L. T_{ws} may serve as T_w as long as $T_{ws} < T_a$, otherwise the lower T_a becomes a better substitute of T_w since T_w must always be lower (unlike T_{ws}) than subhumid T_a due to the energy requirement of evaporation. (b) T_w can be obtained by a combination of its limiting values, the simplest of which is the arithmetic average: $T_w \approx 0.5\ (T_{ws} + T_{wb})$, while keeping the upper limit of T_a. Over areas with sustained air temperature inversions (e.g., Antarctica) T_w is not capped by either T_{ws} or T_a. In such circumstance the CR likely breaks down as the temperature and humidity content of the air may be severely decoupled from the underlying surface owing to strongly stable conditions.

The complementary relationship links the atmospheric humidity to E_p and scales E_w by it to obtain ET, i.e., $ET = F(E_p, E_w)$, where F is a yet undefined function of E_p and E_w. Complementarity exists between E and E_p, since as humidity of the air drops as a response to reduced ET rates, E_p jumps due to a corresponding increase in VPD and, to a smaller degree, to T_a in (3). However, application of the CR is not strictly necessary, as ET rates can directly, rather than indirectly via E_p, be related to the moisture content of the air, once E_w is defined. This direct relationship will be developed and assessed first, followed by a calibration-free formulation of the CR. Performance of the methods and reasons for differences will be discussed.

2. Relating ET Directly to the Moisture Content of the air

A meaningful relationship between ET rates and moisture content of the air, expressed by e_a, must be formulated in dimensionless form. By scaling ET with its maximum attainable value, E_w, to obtain $y = ET/E_w$ and e_a by $e^*(T_w)$ to yield $x = e_a/e^*(T_w)$, two dimensionless variables result with possible values between zero and unity. Since the exact relationship between the two scaled variables is not known, a general polynomial function is sought in the form of

$$y = c_3x^3 + c_2x^2 + c_1x + c_0 \tag{6}$$

by taking into consideration the physical constraints of y and its derivative with respect to x at the limits [*Brutsaert*, 2015]. The four boundary conditions (BCs) are as follows: (i) $y = 1$ when $x = 1$, (ii) $y = 0$ when $x = 0$, (iii) $dy/dx = s_1$ when $x = 1$, and (iv) $dy/dx = s_0$ when $x = 0$. The four BCs result in a system of linear equations for the four unknown parameters (c_i, $i = 0,\ldots,3$), yielding: $c_0 = 0$; $c_1 = s_0$; $c_2 = 3 - 2\,s_0 - s_1$; $c_3 = s_0 + s_1 - 2$. Full saturation of the air over a day or longer periods is a rare occasion due to large-scale advection causing $\alpha > 1$ in (1), thus moving x fast away from its maximum value of unity. The fastest such way is when $(dy/dx)^{-1}$ is at its maximum value at $x = 1$ [i.e., steepest decline for $x(y)$], which yields the minimum dy/dx value of $s_1 = 0$. This transforms (6) into

$$y = (s_0 - 2)x^3 + (3 - 2s_0)x^2 + s_0x \tag{7}$$

containing only one unknown parameter, s_0. Equation (7) is a monotonically increasing function of x (Figure 1) within the [0;1] interval for $0 \le s_0 \le 3$.

2.1. Testing the Direct Approach

Equation (7) was tested at a monthly time step over the contiguous United States with North American Regional Reanalysis (NARR) [*Mesinger et al.*, 2006] radiation, pressure and 10 m wind (u_{10}) data at a spatial resolution of about 30 km and with Parameter-Elevation Regressions on Independent Slopes Model (PRISM) precipitation (P), air, and dew point temperature values [*Daly et al.*, 1994] at a spatial resolution of

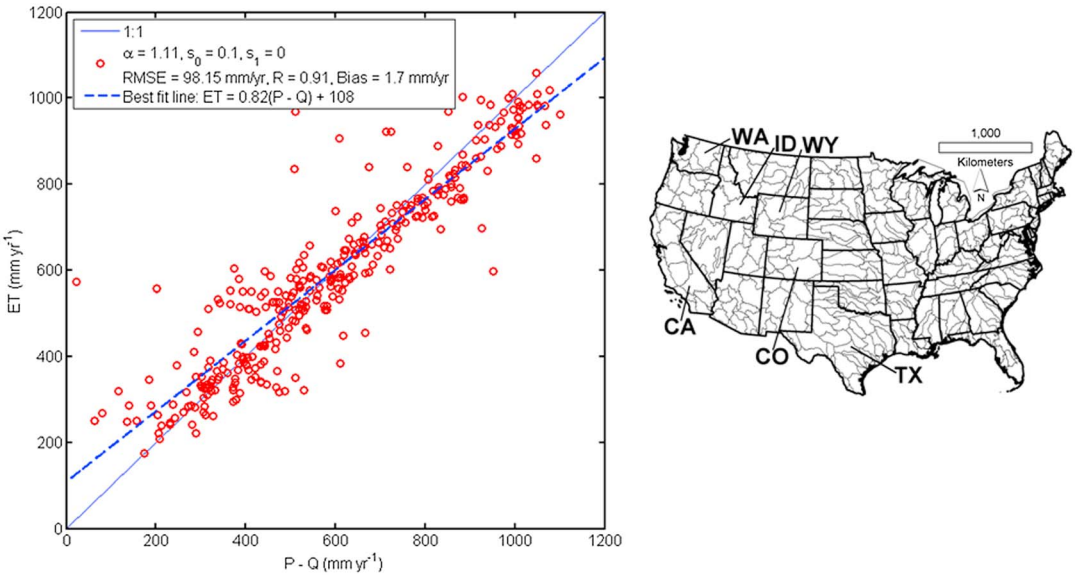

Figure 2. Water balance derived ($P - Q$) and (7)-calibrated long-term (1981–2010) mean annual ET rates for the (right) 334 HUC6-level catchments of the contiguous U.S. $T_w = 0.5(T_{wsM} + T_{wb})$, required by E_w and $e^*(T_w)$. R: linear correlation coefficient, RMSE: root-mean-square error.

4 km. Note that the PRISM T_d values were only available as 30 year normals for 1981–2010 at the time of this research; therefore, the ensuing ET estimation could not be performed on a continuous month-by-month basis, but rather as 30 year normals using similar averages of the input variables. Monthly u_{10} values were transformed to u_2 via $u_2 = u_{10}\,(2/10)^{1/7}$[*Brutsaert*, 1982]. PRISM is widely considered to be the most accurate gridded precipitation data for the contiguous U.S. [Daly *et al.*, 2008]. This and its finer spatial resolution explain the use of PRISM over NARR to obtain P, T_a, and T_d values.

Calibration of the parameters—α in (1) and s_0 in (7)—was performed by a systematic trial and error approach which entails trying out all possible combinations of the parameter values within predefined ranges of the parameters, i.e., $1.1 \le \alpha \le 1.32$ and $0 \le s_0 \le 3$, set apart by similarly predefined small increments. The objective function of calibration consisted of minimizing the root-mean-square error (RMSE) between the mean annual ET estimates and water balance derived ones, the latter obtained as precipitation less United States Geological Survey (USGS) runoff (Q), averaged for the six-level Hydrologic Unit Code (HUC6) catchments across the conterminous US (Figure 2). A repeated calibration with $0 \le s_1 \le 2$ included has confirmed that s_1 is indeed 0, as was concluded above.

As seen in Figure 2, (7) underestimates ET rates at large values and overestimates them at low ones. This overestimation is even more evident in the ET to P ratios, displayed in Figure 3.

While even at a regional scale, it is possible for the mean annual ET rate to exceed precipitation in areas of large-scale irrigation [*Szilagyi*, 2013, 2014b] under a dry and hot climate, such as seen in the Central Valley of California (CA) or the San Juan Valley in south-central Colorado (CO); many of the areas with $ET > 1.2P$ in Figure 3 are fictitious (e.g., the entire area of southwest Texas (TX)), unless the PRISM P values are seriously underestimated, which is unlikely.

Performance of (7) could probably be improved by introducing an additional parameter, following *Brutsaert* [2015]. This is deliberately not performed, because (i) the aim of the present work is the formulation of a calibration-free ET estimation method; (ii) there already exist several CR-based approaches [*Brutsaert*, 2015; *Szilagyi*, 2015; *Szilagyi et al.*, 2016] that require calibration. Instead, the aim is to see if a new, carefully formulated, calibration-free version of the CR can improve upon (7).

3. Derivation of a Calibration-Free CR Approach

The definition of y as ET/E_w and x as $e_a/e^*(T_w)$ is appropriate, because both E_w and T_w are invariable under adiabatic changes of the air in contact with the drying/wetting surface and thus changes in e_a must reflect

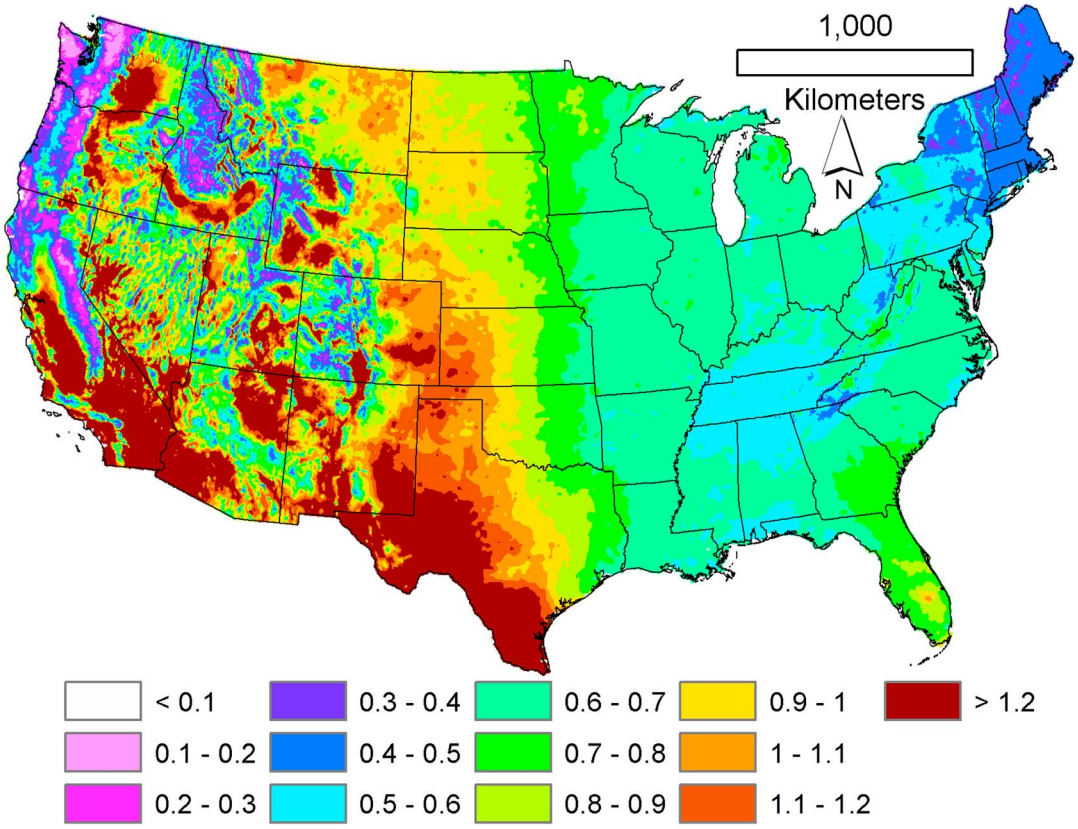

Figure 3. Spatial distribution of the ratio of mean annual ET rates, estimated by (7), and PRISM precipitation values.

changes in ET and vice versa. For any given R_n, y (thus ET) can be zero, provided x (thus e_a) is zero (see (7)) which makes sense. *Brutsaert* [2015] scaled both ET and E_w by E_p, i.e., $y_B = \mathrm{ET}/E_p$ and $x_B = E_w/E_p$. The problem with this definition is that x_B has an ill-defined lower limit since according to BC (ii), y_B must be zero at $x_B = 0$ which is only possible for x_B to reach if either E_p is infinitely large, which is physically unrealistic, or when E_w is zero itself, which is an improbable condition since ET can be zero in a completely dry environment for any given E_w. The situation can easily be mended by introducing the maximum attainable E_p value, E_{pmax}, and scaling x_B as

$$X = \frac{E_{\mathrm{pmax}} - E_p}{E_{\mathrm{pmax}} - E_w} x_B = \frac{E_{\mathrm{pmax}} - E_p}{E_{\mathrm{pmax}} - E_w} \frac{E_w}{E_p} \tag{8}$$

which for any given R_n can yield zero provided E_p reached its maximum, E_{pmax}. (The variable X in (8) is essentially the same as that previously proposed by *Crago et al*. [2016], but written in a different form. Although that work inspired this study, the conceptual development of (8) is largely parallel to, rather than dependent on, *Crago et al*. [2016]). For any R_n and u combination E_p reaches its maximum value when the air becomes void of any moisture. The temperature reached when this maximum E_p happens can easily be defined for adiabatic changes as the $T(e_a = 0) = T_{\mathrm{dry}}$ intercept value of the (T_a, e_a) adiabatic line. The adiabatic line is defined by its two points [*Monteith*, 1981; *Szilagyi*, 2014a]: [T_a, e_a] and [T_{wb}, $e^*(T_{\mathrm{wb}})$] from which T_{dry} can be obtained as

$$T_{\mathrm{dry}} = \frac{e^*(T_{\mathrm{wb}})(T_a - T_{\mathrm{wb}})}{e^*(T_{\mathrm{wb}}) - e_a} + T_{\mathrm{wb}} \tag{9}$$

For adiabatic changes (under $R_n = 0$ valid for the wet bulb of the thermometer) the Bowen ratio equals -1, i.e., $B_o = H/\mathrm{LE} = -1$, which yields an implicit equation for T_{wb}, similar to T_{ws} [*Monteith*, 1981; *Szilagyi*, 2014a]

$$\gamma \frac{T_{\mathrm{wb}} - T_a}{e^*(T_{\mathrm{wb}}) - e^*(T_d)} = -1. \tag{10}$$

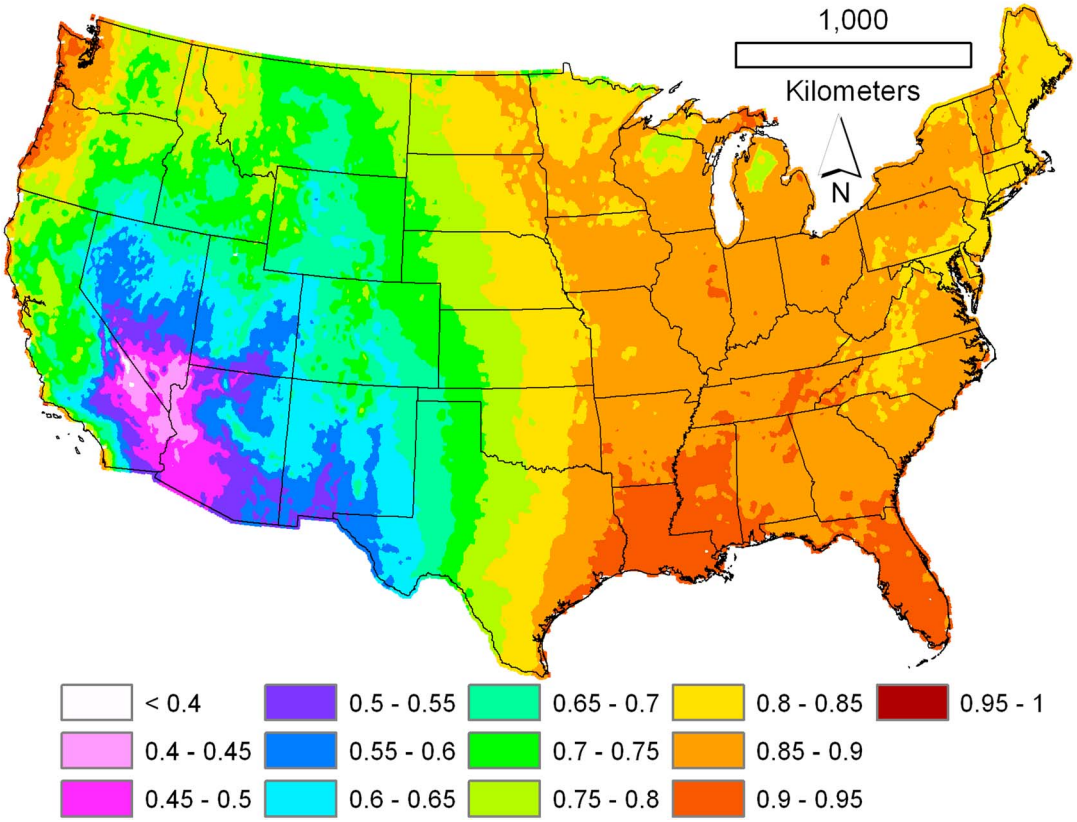

Figure 4. Spatial distribution of the mean annual value of the scaling variable $(E_{\mathrm{pmax}} - E_p)(E_{\mathrm{pmax}} - E_w)^{-1}$.

In humid conditions (10) may yield $T_{\mathrm{wb}} > T_a$ due to measurement errors. In this case an approximate equation may be used [*Szilagyi and Schepers*, 2014], ensuring that $T_{\mathrm{wb}} \leq T_a$

$$T_{\mathrm{wb}} \approx \frac{\gamma T_a + T_d \Delta(T_d)}{\gamma + \Delta(T_d)}. \quad (11)$$

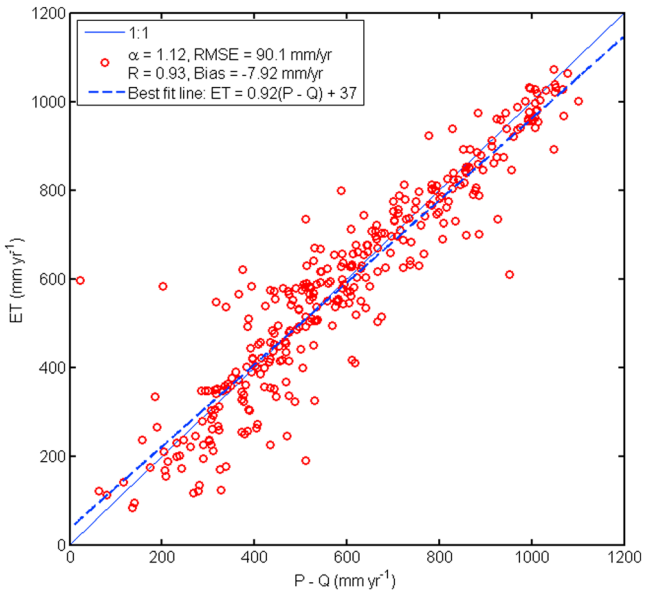

Figure 5. Water balance derived $(P - Q)$ and (13)-calibrated long-term (1981–2010) mean annual ET rates for the 334 HUC6-level catchments of the contiguous U.S.

With T_{dry} obtained and with $e_a = 0$, E_{pmax} can be defined by the Penman equation as

$$E_{p\mathrm{max}} = \frac{\Delta(T_{\mathrm{dry}})}{\Delta(T_{\mathrm{dry}}) + \gamma} R_n + \frac{\gamma}{\Delta(T_{\mathrm{dry}}) + \gamma} f_u e^*(T_{\mathrm{dry}}). \quad (12)$$

E_{pmax} is also invariable to adiabatic changes, similar to E_w and T_w, provided wind conditions remain unchanged. Figure 4 depicts the spatial distribution of the scaling variable $(E_{\mathrm{pmax}} - E_p)(E_{\mathrm{pmax}} - E_w)^{-1}$.

With X defined by (8), the BCs to be used with (6) become (i) $y_B = 1$ when $X = 1$, (ii) $y_B = 0$ when $X = 0$, (iii) $dy_B/dX = 1$ when $X = 1$, and (iv) $dy_B/dX = 0$ when $X = 0$, similar to *Brutsaert* [2015]. The first two BCs are quite self-evident. Justification

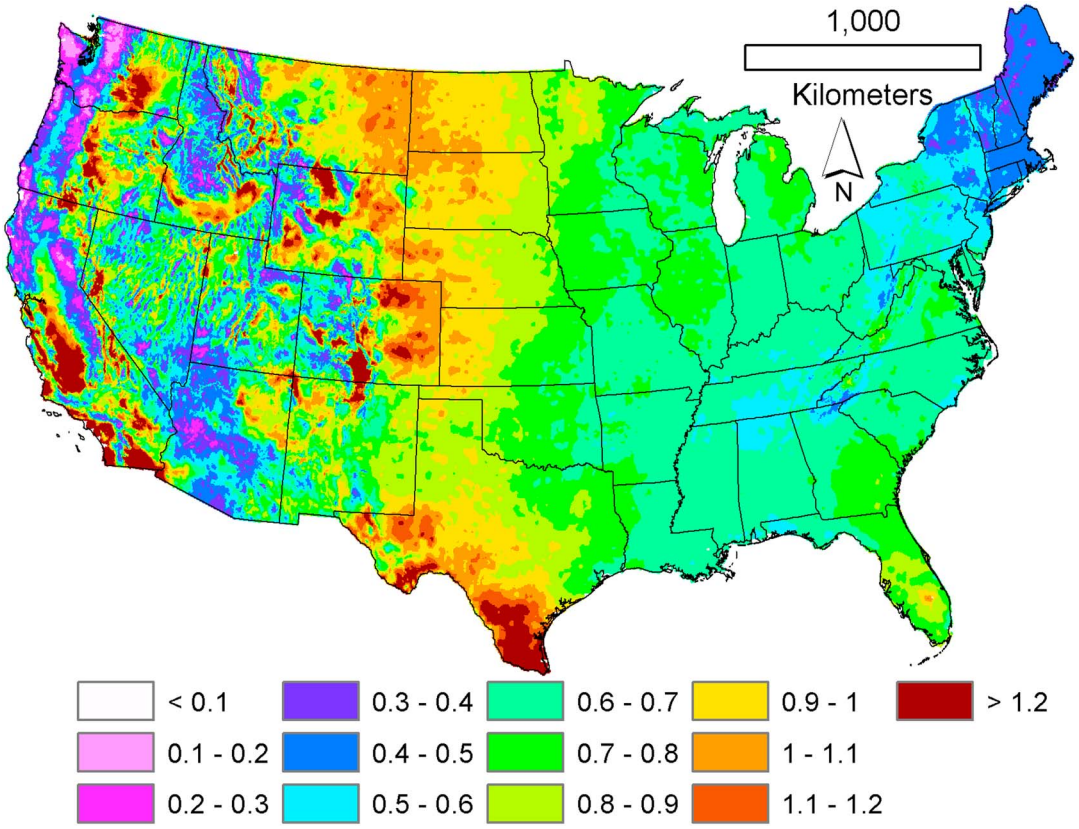

Figure 6. Spatial distribution of the ratio of mean annual ET rates, estimated by calibration of (13), and PRISM precipitation values.

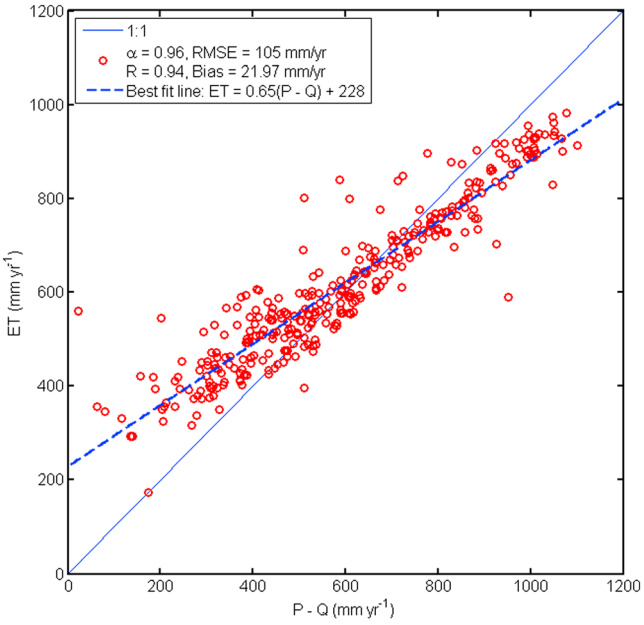

Figure 7. Water balance derived ($P - Q$) and (13)-calibrated long-term (1981–2010) mean annual ET rates, employing $x_B = E_w/E_p$ in place of X, for the 334 HUC6-level catchments of the contiguous U.S.

for (iii) (and (iv)) is the same as was provided by *Brutsaert* [2015] since the change in the scaling variable near $X = 1$ is negligible. BC (iv) is also supported by the experimental data of *Crago et al.* [2016]. The four BCs lead to [*Brutsaert*, 2015]

$$y_B = 2X^2 - X^3 \qquad (13)$$

The best performance of (13) on a monthly basis (similar to the application of (7)) results with the (2)-derived T_w values (limited by T_a) in (1) and $\alpha = 1.12$ (Figure 5).

3.1. Testing the New CR Approach

Figure 6 displays the spatial distribution of the (13)-predicted ET and PRISM P ratios. Areas with predicted ET rates 20% larger than precipitation have shrunk significantly in comparison with Figure 3. Regions with significant large-scale irrigation stand out with their elevated ET rates: the Central and Imperial

Table 1. Mean Values of α From Its Admissible Range of $[1; 1+\gamma/\Delta(T_a)]$, Estimated by (14) for Humid Cells, Employing (2) or (4)[a]

RH (%) >	75	80	85	90	95
$T_{ws} - T_a > 1$ K (# of cells found)	1.29 (110,635)	1.23 (8034)	1.17 (962)	**1.13** (91)	1.09 (4)
$T_{ws} - T_a > 2$ K (# of cells found)	1.23 (65,174)	1.18 (6568)	1.15 (901)	**1.13** (91)	1.09 (4)
$T_{wsM} - T_a > 1$ K (# of cells found)	1.3 (117,781)	1.25 (8140)	1.18 (961)	1.14 (91)	1.1 (4)
$T_{wsM} - T_a > 2$ K (# of cells found)	1.24 (63,725)	1.2 (6376)	1.17 (888)	1.14 (90)	1.1 (4)

[a]The numbers in boldface are the values we accept and use in the calibration free model.

Valleys of California or the San Juan Valley in south-central Colorado. There are areas also where such elevated ET rates are questionable, such as the southern-most part of Texas and the Mojave Desert in Southern California.

For further checking, similar calibration of (13) but with the original variable of $x_B = E_w/E_p$ yields a physically unrealistic α value of 0.96 (Figure 7) and results in a significantly poorer performance which emphasizes the importance of correctly scaling E_p in (8).

In order to have a really useful model, it ought to be calibration-free which may involve a separate method by which the model's parameter values can be set without any calibration, since water balance data may not always be available or may be of poor quality. Over a continental scale, there is a high chance of finding permanently wet areas which help in setting the value of α in (1). By rearranging (1), *Priestley and Taylor* [1972] obtained

$$\alpha = \frac{[\Delta(T_a)+\gamma][e^*(T_{ws}) - e_a]}{\Delta(T_a)\{[e^*(T_{ws}) - e_a] + \gamma(T_{ws} - T_a)\}} \tag{14}$$

where the value of α over extensive wet surfaces must be found within the theoretical limits of $[1; 1+\gamma/\Delta(T_a)]$ [*Priestley and Taylor*, 1972]. For each PRISM cell T_{ws} is estimated either by (2) or (4) (neither limited by T_a) each month but it is not known if the cell is actually wet or not. In order to test for it, cells with (i) relative humidity (RH) value above a set threshold, (ii) T_{ws} value in excess of T_a by a set degree, and (iii) estimated α value that falls within the above interval are chosen. As discussed before, the equilibrium temperature profile over wet surfaces has a mild gradient; thus, cells with $T_{ws} > T_a + 1$ K and $T_{ws} > T_a + 2$ K are sought. RH values of 75, 80, 85, and 90% were chosen. Table 1 lists the so-obtained α values as the arithmetic mean of the cell α values that met the requirements.

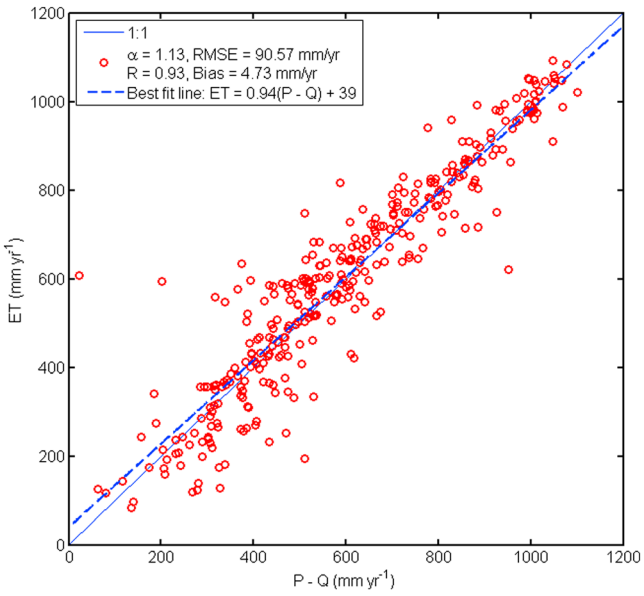

Figure 8. Water balance derived ($P - Q$) and (13)-predicted long-term (1981–2010) mean annual ET rates for the 334 HUC6-level catchments of the contiguous US. Note the absence of calibration.

As seen, the α values approach 1.1 with the humidity of the cells increasing. The 95% RH threshold value resulted in too few cells; thus, the statistically relevant α value of 1.13 (and not 1.14) is accepted considering that the true value must be between 1.14 and 1.1 from the table. Note how close the $\alpha = 1.13$ value is to the calibrated value of 1.12. Figure 8 displays the (13)-predicted ET rates with $\alpha = 1.13$. In comparison with Figure 4, RMSE increased slightly, but R stayed the same; the bias and the best fit equation (in its slope) even improved. It is quite remarkable that a calibration-free ET estimation method without the use of precipitation or runoff rates is able to predict a continental-scale mean annual ET rate (i.e., 537 mm yr^{-1} from water balance) within 1% of the water balance value and also produce a regression slope of practically unity.

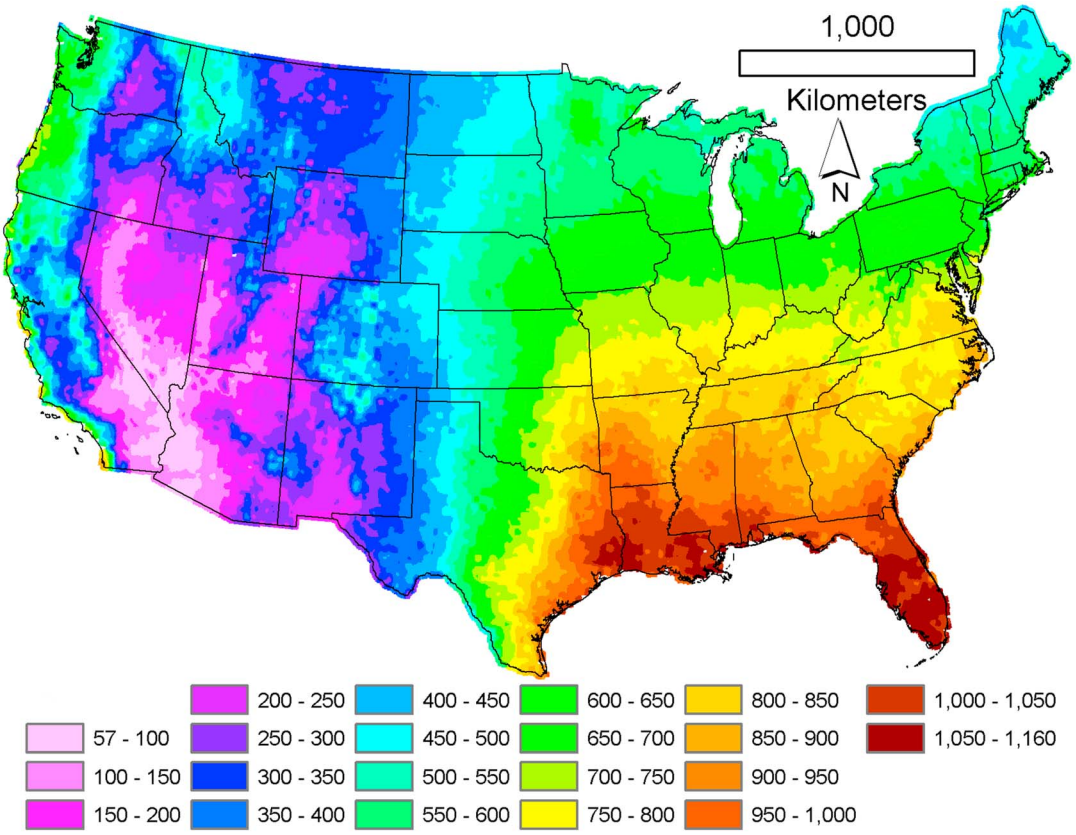

Figure 9. Spatial distribution of the mean annual (1981–2010) ET rates estimated by (13) without calibration (sample mean with the standard deviation and extrema are the following: $\langle ET \rangle = 541 \pm 240$, $ET_{min} = 57$, $ET_{max} = 1152$, all in mm yr^{-1}).

The spatial distribution of the long-term mean annual ET rates is seen in Figure 9. The highest ET rates, as expected, can be found along the Gulf of Mexico, Louisiana, and Florida, being the wettest states, while Nevada the driest. The ET to P ratios are shown in Figure 10. The areas with $ET > 1.2P$ only slightly increased over that in Figure 6. Most of these areas are connected to large-scale irrigation schemes in regions with $P < 400$ mm yr^{-1} as far north as Wyoming (WY), Idaho (ID), and Washington (WA) (Figure 11). The only exception is the southern-most part of Texas.

The spatial distribution of the ratios of HUC6-averaged ET estimates and those derived by water balance demonstrates (Figure 12) that over the vast majority (>80%) of the 334 HUC6 watersheds, estimated ET rates are within 20% of the water balance derived ones (turquoise and green).

Finally, sensitivity analysis indicates (Figure 13) that (13) is quite sensitive to the parameter value of the Priestley-Taylor α, but this is true for any CR-based method [*Szilagyi et al*., 2016]; it is not the result of the nonlinearity of (13).

4. Discussion and Summary

Up until the publication of *Han et al*. [2012] and *Brutsaert* [2015], not much thought was given to how the CR behaves at extremes of the ET values, $0 \le ET \le E_w$. The CR, e.g., in the classical Advection-Aridity model of *Brutsaert and Stricker* [1979], was thought to be symmetric, i.e., $y_B = 2x_B - 1$, and later a constant (d) was introduced [*Kahler and Brutsaert*, 2006] to account for the frequently observed asymmetry in the relationship, i.e., $y_B = (1 + d)\, d^{-1}\, x_B - d^{-1}$. However, the CR, up until now, has suffered from ill-defined scaling of E_p as it has always been related to its minimum value only, i.e., to E_w. For example, in the symmetric CR one has $E_w - ET = E_p - E_w$, while in the asymmetric one it becomes $E_w - ET = (E_p - E_w)/d$. An appropriate scaling for E_p should account for its physically based limits, i.e., $E_w \le E_p \le E_{pmax}$, just as the ET/E_w does for ET. The result becomes

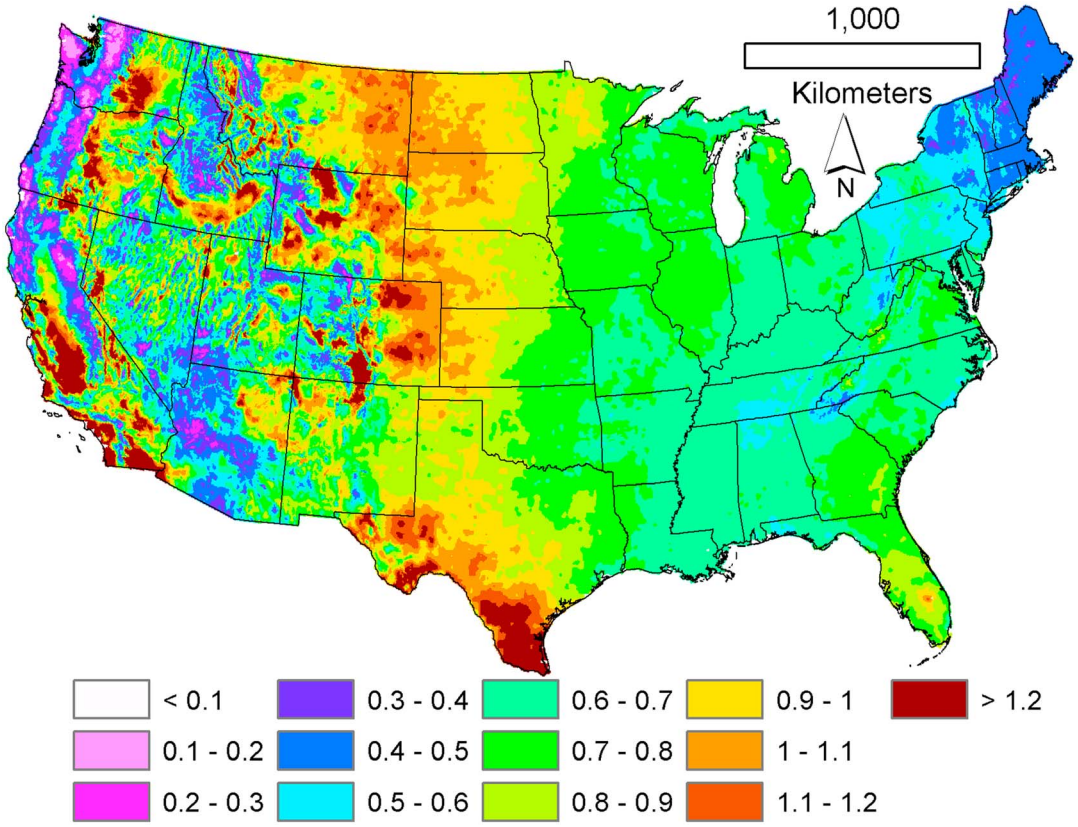

Figure 10. Spatial distribution of the ratio of mean annual ET rates, estimated by (13) without calibration, and PRISM precipitation values.

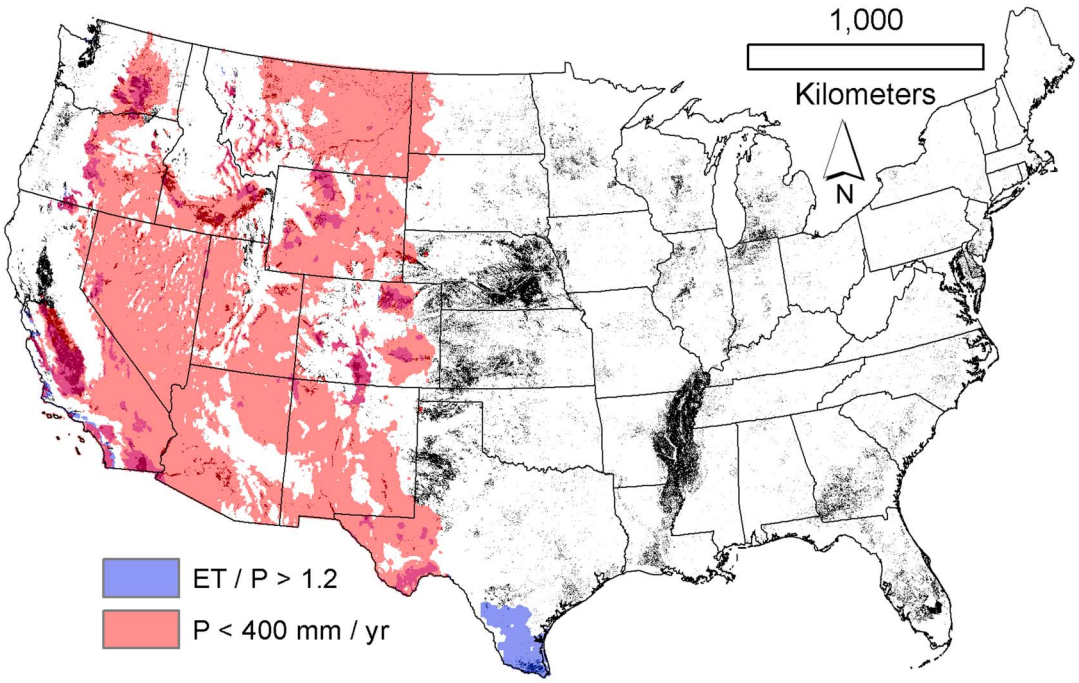

Figure 11. Spatial distribution of irrigated areas denoted by black dots [after *Brown and Pervez*, 2014]. With the exception of Southern Texas, the $P < 400$ mm yr^{-1} and ET/$P > 1.2$ conditions overlap (magenta-colored areas), often in regions of wide-spread irrigation (black dots in areas of magenta).

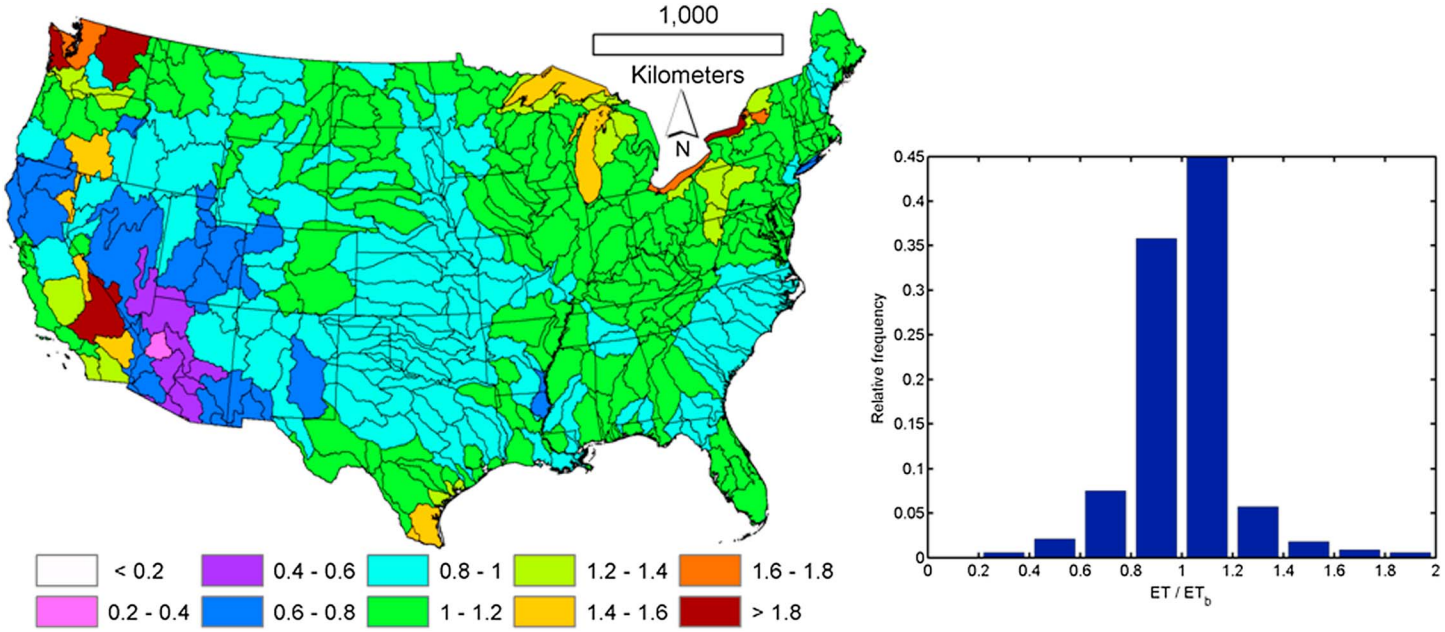

Figure 12. Spatial distribution of the ratio of HUC6-level watershed averaged ET estimates and the water balance derived (ET_b) values as the difference of precipitation and runoff.

$$y = \frac{ET}{E_w} = g\left(\frac{E_{\mathrm{pmax}} - E_p}{E_{\mathrm{pmax}} - E_w}\right) = g(x^*) \tag{15}$$

where g denotes a yet unspecified functional relationship, another functional relationship, f, can equally be sought by multiplying both y and the argument of g with $x_B = E_w/E_p$ yielding $\mathrm{ET}/E_p = y_B = f(\frac{E_{\mathrm{pmax}}-E_p}{E_{\mathrm{pmax}}-E_w} x_B) = f(X)$. Applying the polynomial approach (equation (6)) and considering the behavior of the scaled variables at their extreme values leads to $f(X) = 2X^2 - X^3$. Note that a direct calibration of s_0, s_1, and α in a similar polynomial approach of g in (15) (results not displayed) did not improve (best fit slope of 0.81) upon the calibration-free application of $f(X)$ in (13). Neither did similar calibration of the slope values, s_0, s_1, and α for f in the case when $(E_{\mathrm{pmax}} - E_p)(E_{\mathrm{pmax}} - E_w)^{-1}$ was replaced by the vapor pressure ratios in (13) (best fit slope of 0.88, not displayed).

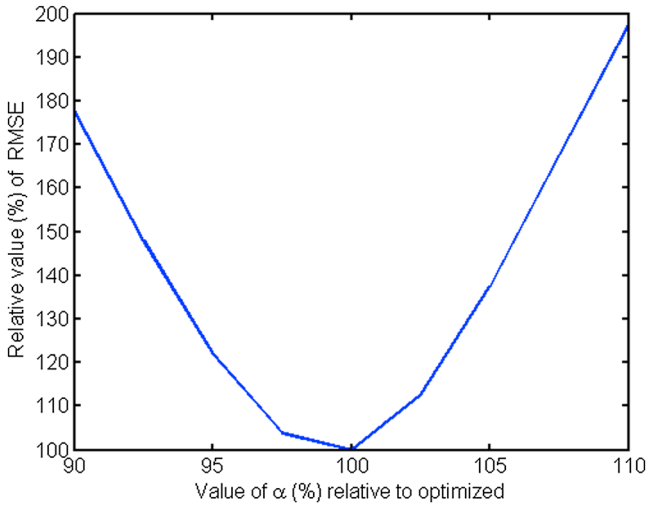

Figure 13. Sensitivity of (13) to the value of the Priestley-Taylor α.

The explanation is that y_B (= ET/E_p) is a more sensitive variable than y (= ET/E_w), since for y_B, ET, and E_p change in opposite directions during drying/wetting periods, while for y, E_w remains constant under adiabatic changes leading to a more sluggish response to water availability and thus manifesting in mild best fit slope of the regression plot. Similarly, E_p in the $(E_{\mathrm{pmax}} - E_p)(E_{\mathrm{pmax}} - E_w)^{-1}$ term is more responsive to changes in wetness than e_a itself because on top of the e_a changes (via the VPD term of (3)) it also incorporates the temperature change over the drying/wetting surface (note the different temperatures in E_w and E_p).

The correct scaling of E_p and the specification of E_{pmax} in each computational

step (monthly here) is the main contribution of the present work, together with a unique estimation of the Priestley-Taylor α parameter, using continental-scale data. The present calibration-free CR relationship yields ET estimates on par with the latest land surface model (LSM) results [*Sheffield et al*., 2012] utilizing only basic atmospheric data, unlike LSMs that in addition require information on vegetation and soil type and keep a soil moisture budgeting. The current calibration-free approach improves upon recent, two-parameter formulations of the CR by *Szilagyi* [2015] and *Szilagyi et al*. [2016] using the same data set.

The novel estimation of the Priestley-Taylor α parameter introduced here is independent of the CR model. As it involves extensive saturated areas, it works, in general, with continental-scale data sets. The calibration-free CR model with its minimal (T_a, T_d, R_n, u) data requirements, coupled with a model-independent calculation of α, presents itself as a convenient tool for routinely estimating ET rates over extensive areas, such as continents. The model-derived ET rates may also serve as independent, calibration-free estimates of continental or global-scale latent heat fluxes by which similar values of different LSM versions together with their coupled climate models can be calibrated and/or validated, especially under future climate scenarios when measurements of the surface fluxes are not available.

Notation

α	Priestley-Taylor coefficient, dimensionless.
γ	psychrometric constant, hPa K^{-1}.
Δ	slope of the saturation vapor pressure curve, hPa K^{-1}.
Δ^{wb}	slope of the saturation vapor pressure curve at T_{wb}, hPa K^{-1}.
ρ	water density, kg m^{-3}.
B_o	Bowen ratio, dimensionless.
c_p	specific heat of air at constant air pressure, J kg^{-1} hPa^{-1}.
e_a	actual vapor pressure, hPa.
e^*	saturation vapor pressure, hPa.
E_p	potential evaporation rate, mm d^{-1}.
E_{pmax}	dry-environment potential evaporation rate, mm d^{-1}.
E_w	wet-environment evaporation rate, mm d^{-1}.
ET	actual evaporation rate, mm d^{-1}.
ET_b	water balance derived actual evaporation rate, mm yr^{-1}.
f_u	wind function, mm d^{-1} hPa^{-1}.
H	surface sensible heat flux, W m^{-2};
L	latent heat of vaporization, J kg^{-1}.
LE	surface latent heat flux, W m^{-2}.
p	air pressure, hPa.
P	mean annual precipitation rate, mm yr^{-1}.
Q	mean annual streamflow rate, mm yr^{-1}.
Q_n	surface net radiation, W m^{-2}.
R_n	surface net radiation in water equivalent of mm d^{-1}.
RH	relative humidity, %.
T	air temperature, °C.
T_a	air temperature, K.
T_d	dew point temperature, K.
T_{dry}	dry-environment air temperature, K.
T_w	wet-environment air temperature, K.
T_{wb}	wet-bulb temperature, K.
T_{ws}	wet-surface temperature, K.
T_{wsM}	wet-surface temperature from Monteith-Penman parameterization, K.
u_2, u_{10}	mean horizontal wind speed at 2 and 10 m, respectively, above the ground, m s^{-1}.
VPD	vapor pressure deficit, hPa.

Acknowledgments

This research was supported in part by NIFA grant IDA01476. The authors are grateful for the two anonymous reviewers whose comments led to important revisions. All data used in this study are publicly available from the following sites: waterwatch.usgs.gov (runoff data), www.prism.oregonstate.edu (PRISM data), www.esrl.noaa.gov/psd/data/gridded/data.narr.html (NARR data). Modeled spatially distributed data of this study are available from the corresponding author upon request.

References

Berbery, E. H., Y. Luo, K. E. Mitchell, and A. K. Betts (2003), Eta model estimated land surface processes and the hydrologic cycle of the Mississippi basin, *J. Geophys. Res.*, *108*(D2), 28852, doi:10.1029/2002JD003192.

Bouchet, R. J. (1963), Evapotranspiration reelle, evapotranspiration potentielle, et production agricole, *Annal. Agronom.*, *14*, 743–824.

Brown, J. F., and M. S. Pervez (2014), Merging remote sensing data and national agricultural statistics to model change in irrigated agriculture, *Agric. Syst.*, *127*, doi:10.1016/j.agsy.2014.01.004.

Brutsaert, W. (1982), *Evaporation Into the Atmosphere: Theory, History and Applications*, D. Reider, Dordrecht, Netherlands.

Brutsaert, W. (2015), A generalized complementary principle with physical constraints for land-surface evaporation, *Water Resour. Res.*, *51*, 8087–8093, doi:10.1002/2015WR017720.

Brutsaert, W., and M. B. Parlange (1998), Hydrologic cycle explains the evaporation paradox, *Nature*, *396*, 30.

Brutsaert, W., and H. Stricker (1979), An advection-aridity approach to estimate actual regional evapotranspiration, *Water Resour. Res.*, *15*, 443–449, doi:10.1029/WR015i002p00443.

Campoy, A., A. Ducharne, F. Cheruy, F. Hourdin, J. Polcher, and J. C. Dupont (2013), Response of land surface fluxes and precipitation to different soil bottom hydrological conditions in a general circulation model, *J. Geophys. Res. Atmos.*, *118*, 10,725–10,739, doi:10.1002/jgrd.50627.

Chen, F., Z. Janjic, and K. Mitchell (1997), Impact of atmospheric surface-layer parameterizations in the new land-surface scheme of the NCEP mesoscale Eta model, *Boundary Layer Meteorol.*, *85*, 39–421.

Crago, R., J. Szilagyi, R. Qualls, and J. Huntington (2016), Rescaling the complementary relationship for land surface evaporation, *Water Resour. Res.*, *52*, 8461–8471, doi:10.1002/2016WR019753.

Culf, A. D. (1994), Equilibrium evaporation beneath a growing convective boundary layer, *Boundary Layer Meteorol.*, *70*, 37–49.

Daly, C., R. P. Neilson, and D. L. Phillips (1994), A statistical topographic model for mapping climatological precipitation over mountainous terrain, *J. Appl. Meteorol.*, *33*, 140–158.

Daly, C., M. Halbleib, J. I. Smith, W. P. Gibson, M. K. Doggett, G. H. Taylor, J. Curtis, and P. P. Pasteris (2008), Physiographically sensitive mapping of climatological temperature and precipitation across the conterminous United States, *Int. J. Clim.*, *28*(15), 2031–2064. doi:10.1002/joc.1688.

Davenport, D. C., and J. P. Hudson (1967), Changes in evaporation rates along a 17-km transect in the Sudan Gezira, *Agric. Meteorol.*, *4*, 339–352.

de Bruin, H. A. R. (1983), A model for the Priestley-Taylor parameter α, *J. Clim. Appl. Meteorol.*, *22*, 572–580.

Diro, G. T., L. Sushama, A. Martynov, D. I. Jeong, D. Verseghy, and K. Winger (2014), Land-atmosphere coupling over North America in CRCM5, *J. Geophys. Res. Atmos.*, *119*, 11,955–11,972, doi:10.1002/2014JD021677.

Han, S., H. Hu, and F. Tian (2012), A nonlinear function approach for the normalized relationship evaporation model, *Hydrol. Process.*, *26*, 3973–3981, doi:10.1002/hyp.8414.

Heerwaarden, C. C., J. V. Arellano, A. F. Moene, and A. A. M. Holtslag (2009), Interactions between dry-air entrainment, surface evaporation and convective boundary-layer development, *Q. J. R. Meteorol. Soc.*, *135*, 1277–1291.

Huntington, J., J. Szilagyi, S. Tyler, and G. Pohll (2011), Evaluating the complementary relationship for estimating evapotranspiration from arid shrublands, *Water Resour. Res.*, *47*, W05533, doi:10.1029/2010WR009874.

Kahler, D. M., and W. Brutsaert (2006), Complementary relationship between daily evaporation in the environment and pan evaporation, *Water Resour. Res.*, *42*, W05413, doi:10.1029/2005WR004541.

Koster, R. D., and M. J. Suarez (1996), *Energy and Water Balance Calculations in the Mosaic LSM*, NASA Tech. Memo, NASA TM-104606, 9, 60, Goddard Space Flight Cent, Greenbelt, Md.

Lang, A. R. G., G. N. Evans, and P. Y. Ho (1974), The influence of local advection on evapotranspiration from irrigated rice from a semi-arid region, *Agric. Meteorol.*, *13*, 5–13.

Lavers, D. A., G. Villarini, R. P. Allan, E. F. Wood, and A. J. Wade (2012), The detection of atmospheric rivers in atmospheric reanalyses and their links to British winter floods and the large-scale climatic circulation, *J. Geophys. Res.*, *117*, D20106, doi:10.1029/2012JD018027.

Lhomme, J. P. (1997), A theoretical basis for the Priestley-Taylor coefficient, *Boundary Layer Meteorol.*, *82*, 179–191.

Liang, X., D. P. Lettenmaier, E. F. Wood, and S. J. Burges (1994), A simple hydrologically based model of land surface water and energy fluxes for GCMs, *J. Geophys. Res.*, *99*(D7), 14,415–14,428, doi:10.1029/94JD00483.

Ma, N., Y. Zhang, C.-Y. Xu, and J. Szilagyi (2015), Modeling actual evapotranspiration with routine meteorological variables in the data-scarce region of the Tibetan Plateau: Comparisons and implications, *J. Geophys. Res. Biogeosci.*, *120*, 1638–1657, doi:10.1002/2015JG003006.

Mesinger, F., et al. (2006), North American regional reanalysis, *Bull. Am. Meteorol. Soc.*, *87*, 343–360.

Monteith, J. L. (1965), Evaporation and environment, in *Proceedings of the 19th Symposium of the Society for Experimental Biology*, pp. 205–233, Cambridge Univ. Press, Cambridge, New York.

Monteith, J. L. (1981), Evaporation and surface temperature, *Q. J. R. Meteorol. Soc.*, *107*, 1–27.

Morton, F. I. (1983), Operational estimates of areal evapotranspiration and their significance to the science and practice of hydrology, *J. Hydrol.*, *66*, 1–76.

Penman, H. L. (1948), Natural evaporation from open water, bare soil, and grass, *Proc. R. Soc. London, Ser. A*, *193*, 120–146.

Peterson, T. C., V. S. Golubev, and P. Y. Groisman (1995), Evaporation losing its strength, *Nature*, *377*, 687–688.

Phillips, T. J., and S. A. Klein (2013), Land-atmosphere coupling manifested in warm-season observations on the U.S. southern great plains, *J. Geophys. Res. Atmos.*, *119*, 509–528, doi:10.1002/2013JD020492.

Priestley, C. H. B., and R. J. Taylor (1972), On the assessment of surface heat flux and evaporation using large-scale parameters, *Mon. Weather Rev.*, *100*(2), 81–92.

Sheffield, J., and E. F. Wood (2007), Characteristics of global and regional drought, 1950–2000: Analysis of soil moisture data from off-line simulation of the terrestrial hydrologic cycle, *J. Geophys. Res.*, *112*, D17115, doi:10.1029/2006JD008288.

Sheffield, J., B. Livneh, and E. F. Wood (2012), Representation of terrestrial hydrology and large-scale drought of the continental United States from the North American Regional Reanalysis, *J. Hydrometeor.*, *13*, 856–876, doi:10.1175/JHM-D-11-065.1.

Swenson, S. C., and D. M. Lawrence (2014), Assessing a dry surface layer-based soil resistance parameterization for the Community Land Model using GRACE and FUXNET-MTE data, *J. Geophys. Res. Atmos.*, *119*, 10,299–10,312, doi:10.1002/2014JD022314.

Szilagyi, J. (2013), Recent updates of the Calibration-Free Evapotranspiration Mapping (CREMAP) method, in *Evapotranspiration—An Overview*, edited by S. Alexandris, INTECH, Rijeka, Croatia. [Available at http://www.intechopen.com/books/ evapotranspiration-an-overview.]

Szilagyi, J. (2014a), Temperature corrections in the Priestley-Taylor equation of evaporation, *J. Hydrol.*, *519*, 455–464, doi:10.1016/j.jhydrol.2014.07.040.

Szilagyi, J. (2014b), MODIS-aided water-balance investigations in the Republican River basin, USA, *Periodica Polytech.-Civil Engin.*, *58*(1), 33–46.
Szilagyi, J. (2015), Complementary-relationship-based 30 year normals (1981–2010) of monthly latent heat fluxes across the contiguous United States, *Water Resour. Res.*, *51*, 9367–9377, doi:10.1002/2015WR017693.
Szilagyi, J., and A. Schepers (2014), Coupled heat and vapor transport: The thermostat effect of a freely evaporating land surface, *Geophys. Res. Lett.*, *41*, 435–441, doi:10.1002/2013GL058979.
Szilagyi, J., and J. Jozsa (2008), New findings about the complementary relationship-based evaporation estimation methods, *J. Hydrol.*, *354*(1-4), 171–186.
Szilagyi, J., A. Kovacs, and J. Jozsa (2011), A calibration-free evapotranspiration mapping (CREMAP) technique, in *Evapotranspiration*, edited by L. Labedzki, INTECH, Rijeka, Croatia. [Available at http://www.intechopen.com/books/show/title/evapotranspiration.]
Szilagyi, J., R. Crago, and R. J. Qualls (2016), Testing the generalized complementary relationship of evaporation with continental-scale long-term water-balance data, *J. Hydrol.*, *540*, 914–922.
Thornthwaite, C. W., and J. R. Mather (1955), *The Water Balance*, *Drexel Institute of Technology*, vol. 8, Climatological Laboratory Publication, Philadelphia, Pa.
Wang, K., and R. E. Dickinson (2012), A review of global terrestrial evapotranspiration: observation, modeling, climatology, and climatic variability, *Rev. Geophys.*, *50*, RG2005, doi:10.1029/2011RG000373.
Wu, R., Q. Ge, X. Zhan, F. Guan, and S. Yao (2014), Drought monitoring based on simulated surface evapotranspiration by BEPS model, *J. Nat. Disasters*, *23*(1), 7–16.
Xia, Y., M. B. Ek, C. D. Peters-Lidard, D. Mocko, M. Svoboda, J. Sheffield, and E. F. Wood (2014), Application of USDM statistics in NLDAS-2: Optimal blended NLDAS drought index over the continental United States, *J. Geophys. Res. Atmos.*, *119*, 2947–2965, doi:10.1002/2013JD020994.
Zhang, J., W.-C. Wang, and L. R. Leung (2008), Contribution of land-atmosphere coupling to summer climate variability over the contiguous United States, *J. Geophys. Res.*, *113*, D22109, doi:10.1029/2008JD010136.
Zhang, Y., C. Liu, Y. Tang, and Y. Yang (2007), Trends in pan evaporation and reference and actual evapotranspiration across the Tibetan Plateau, *J. Geophys. Res.*, *112*, D12110, doi:10.1029/2006JD008161.